

Counteraction of antibiotic production and degradation stabilizes microbial communities

Eric D. Kelsic¹, Jeffrey Zhao¹, Kalin Vetsigian² & Roy Kishony^{1,3}

A major challenge in theoretical ecology is understanding how natural microbial communities support species diversity^{1–8}, and in particular how antibiotic-producing, -sensitive and -resistant species coexist^{9–15}. While cyclic ‘rock–paper–scissors’ interactions can stabilize communities in spatial environments^{9–11}, coexistence in unstructured environments remains unexplained^{12,16}. Here, using simulations and analytical models, we show that the opposing actions of antibiotic production and degradation enable coexistence even in well-mixed environments. Coexistence depends on three-way interactions in which an antibiotic-degrading species attenuates the inhibitory interactions between two other species. These interactions enable coexistence that is robust to substantial differences in inherent species growth rates and to invasion by ‘cheating’ species that cease to produce or degrade antibiotics. At least two antibiotics are required for stability, with greater numbers of antibiotics enabling more complex communities and diverse dynamic behaviours ranging from stable fixed points to limit cycles and chaos. Together, these results show how multi-species antibiotic interactions can generate ecological stability in both spatially structured and mixed microbial communities, suggesting strategies for engineering synthetic ecosystems and highlighting the importance of toxin production and degradation for microbial biodiversity.

Antibiotic-producing species are common in natural microbial communities^{13,17,18}. Ecological models of antibiotics typically assume pairwise species relationships, where antibiotic producers inhibit sensitive species more than resistant species. These pairwise inhibitory interactions, combined with costs for production and resistance, can lead to relationships of cyclic dominance among species (for example, rock–paper–scissors games), which can support coexistence in spatial environments^{9–11} beyond the limit set by competitive exclusion^{4,5}. However, such pairwise interaction models lead to coexistence through the separation of species into distinct spatial domains, whereas in nature antibiotic-producing, -resistant and -sensitive species appear to intermix even at very small length scales^{17,19}. Furthermore, species communities stabilized through pairwise antibiotic interactions are not resilient to the high level of species dispersal expected in nature^{12,16}. Understanding how multiple antibiotic-producing species coexist despite dispersal remains an open question.

The inhibitory interaction between an antibiotic-producing species and an antibiotic-sensitive species can be attenuated by the presence of a third ‘modulator’ species (Fig. 1a). One established mechanism for antibiotic attenuation is enzymatic degradation²⁰, a common mechanism for antibiotic resistance²¹. In principle, a modulator species could also intensify inhibitory interactions between two species^{22,23}, for example by inducing antibiotic production. However, when testing for such interactions among a collection of soil isolates using a three-species interaction assay (Fig. 1b), we observed that intensification was rare, while attenuation was common (Extended Data Figs 1, 2 and Extended Data Table 1). Realizing that such three-way attenuating interactions commonly occur among natural species motivated us to

explore their impact on ecological dynamics. We focus on antibiotic attenuation caused by degradation, which we observed experimentally (Extended Data Figs 1d and 2c), but our analysis can be generalized to other attenuation mechanisms such as antibiotic suppression²⁴. It is known that antibiotic-degrading species can coexist together with sensitive species when an antibiotic is provided externally^{25–27}. However, when antibiotics are produced by the species themselves, these two-species communities are no longer stabilized by degradation^{27,28}. The impact of antibiotic-degrading species on the stability of larger ecosystems has not been explored.

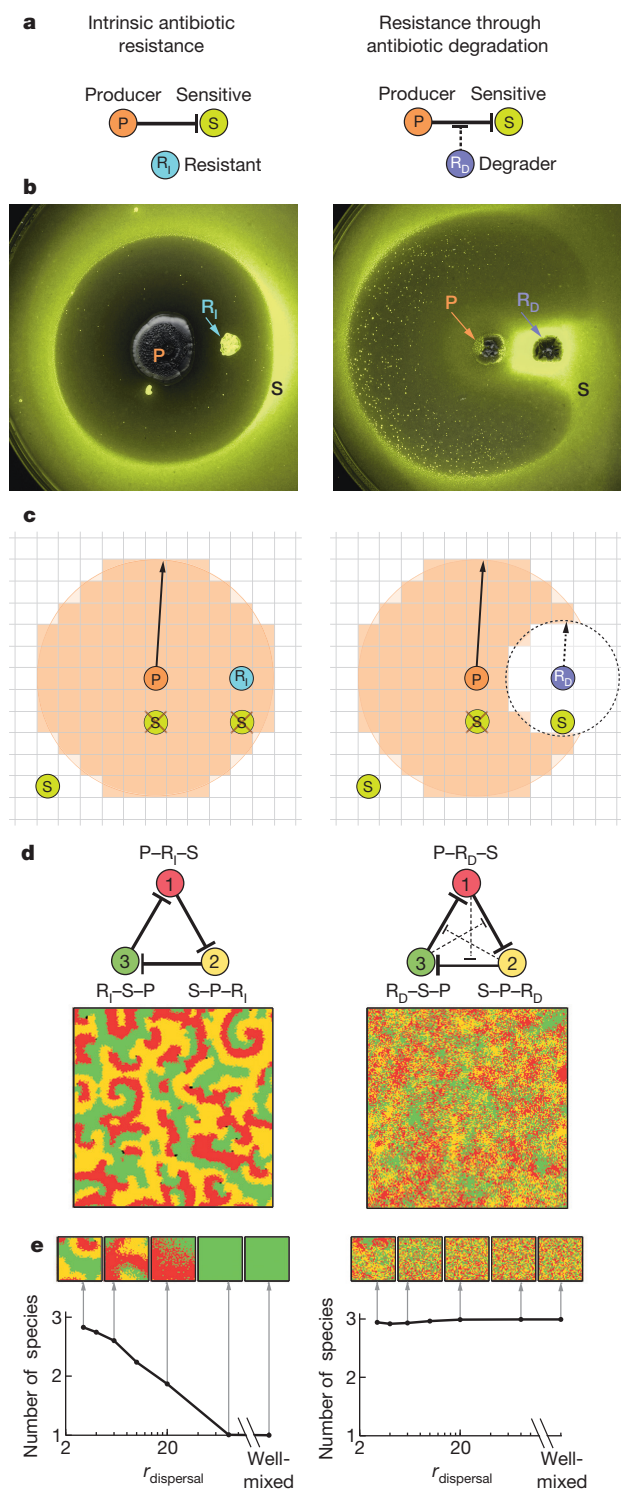
We investigated how antibiotic-degrading species affect the dynamics of microbial communities containing antibiotic producers by modifying a classical spatial model of antibiotic-mediated interactions. As in previous spatial models of antibiotic inhibition^{9–12}, we consider antibiotic-producing, -sensitive or -resistant species phenotypes. However, unlike in previous models, in addition to intrinsic resistance we also consider resistance through antibiotic degradation (Fig. 1a, b). Antibiotic-degrading species remove antibiotics from nearby locations, thereby protecting not only themselves but also neighbouring species. The simulations are performed on a grid (Fig. 1c), with each simulation step consisting of: production of antibiotics around antibiotic-producing species (within area of size K_P), removal of antibiotics near antibiotic-degrading species (within area of size K_D), killing of antibiotic-sensitive species within the antibiotic zones, and finally colonization of empty regions on a new grid by randomly choosing surviving species within a given dispersal radius, $r_{\text{dispersal}}$ (Extended Data Fig. 3; Methods).

In these spatial inhibition-zone models, communities with intrinsic resistance and with resistance through antibiotic degradation result in dramatically different patterning and robustness to dispersal. We simulated a simple three-species and three-antibiotic network that exhibits cyclic dominance. Consistent with previous studies^{9–12}, pairwise interactions among intrinsically resistant species result in coexistence of all three species through single-species domains that continually chase each other around the grid (Fig. 1d, left). However, we found that three-way interactions created by antibiotic degradation lead to tight intermixing of species (Fig. 1d, right). This fine-scale intermixing allowed us to investigate whether a spatial environment was necessary for the coexistence of these antibiotic-degrading communities. Spatial structure is needed for coexistence in pairwise antibiotic-interaction models^{9–12}, and diversity of the community with intrinsic resistance collapses when the dispersal radius increases (Fig. 1e, left; Supplementary Videos 1–5). In contrast, the antibiotic-degrading community maintains diversity across any level of dispersal, even with complete mixing between time steps (Fig. 1e, right; Supplementary Videos 6–10).

We characterized the stability of these communities with respect to model parameters by considering the analytical limit of an infinitely large environment with complete mixing between time steps ($r_{\text{dispersal}} \rightarrow \infty$; a ‘mixed inhibition-zone model’; Methods). Considering different initial species abundances, the community with

¹Department of Systems Biology, Harvard Medical School, Boston, Massachusetts 02115, USA. ²Department of Bacteriology and Wisconsin Institute for Discovery, University of Wisconsin-Madison, Madison, Wisconsin 53715, USA. ³Department of Biology and Department of Computer Science, Technion-Israel Institute of Technology, Haifa 3200003, Israel.

intrinsically resistant species coexists only at a single unstable fixed point; starting in any other initial condition leads to extinction of all but one species (Fig. 2a, left). In contrast, the community with antibiotic degradation coexists with a stable fixed point and a large basin of attraction (Fig. 2a, right). Moreover, antibiotic degradation enables stable communities to form despite large differences in inherent species growth rates (g_1, g_2, g_3 ; Fig. 2b, right). Thus, even in environments with complete mixing, the interplay of antibiotic production and degradation leads to coexistence that is robust to large perturbations of species abundances and substantial differences in inherent growth rates.



Community stability is maximized at intermediate levels of antibiotic degradation (Fig. 2c and Extended Data Fig. 4a). Levels of degradation that are too high mostly eliminate the effects of the antibiotics, after which inherent growth rate differences lead to one species taking over. Levels of degradation that are too low do not allow coexistence, as expected, since $K_D = 0$ is equivalent to intrinsic antibiotic resistance. Stability is therefore maximal at intermediate levels of degradation where a negative feedback can operate, such that increased abundance of a given species results in its increased inhibition (Extended Data Fig. 4b–d). In contrast, stability is maximal at high levels of antibiotic production (K_P). Thus, strong antibiotic production can stabilize diversity when combined with intermediate levels of antibiotic degradation.

Production and degradation of multiple antibiotics also leads to robust coexistence in a well-mixed chemostat setting. We modelled the cyclic three-species, three-antibiotic interaction network using a single resource chemostat model. While these models are inherently unstable with intrinsic resistance, implementing resistance through enzymatic degradation of antibiotics allows coexistence of all species through stable fixed points or limit cycles (Methods). As in the inhibition-zone model, stability occurs despite inherent growth rate differences among species and was strengthened at high levels of production and intermediate levels of degradation (Extended Data Fig. 5a). We also observed robust coexistence for different forms of antibiotic inhibition functions and when inhibitory interactions are diffuse²⁹, that is, when all species have finite sensitivity to each antibiotic (Extended Data Fig. 5b). This generality with respect to different models, assumptions, and parameter values suggests that the counteraction of antibiotic production and degradation can support coexistence in a wide variety of settings.

These three-species ecosystems are also stable with respect to cheaters; that is, they resist invasion by species that gain a small growth advantage by ceasing production or degradation of antibiotics. We consider two types of cheating species: those that stop producing antibiotics and revert to intrinsic resistance while enjoying the production of antibiotics by their parental species, and those that stop degrading antibiotics to become antibiotic sensitive, yet still enjoy protection by their parental species (Fig. 3a). Starting with a stable three-species community, we simulated potential cheater invasion by adding a small amount of a cheater species derived from one of the existing species. We calculated the final abundance of a cheater once the community reached steady state while varying the growth advantage of the cheater compared to its parent: $g_i^{\text{cheater}} = (1 + \epsilon)g_i$. We assume that each species has a different inherent growth rate, $g_1 < g_2 < g_3$. For small

Figure 1 | Replacing intrinsic antibiotic resistance with degradation-based resistance generates community robustness to species dispersal. **a**, Pairwise interactions among antibiotic-producing (P), -sensitive (S) and intrinsically resistant (R_i) species are compared to three-way interactions where the sensitive species can be protected by an antibiotic degrading species (R_d). **b**, Images of a YFP-labelled probe *Escherichia coli* strain (S, yellow-green) growing in the presence of two *Streptomyces* colonies. The inhibition of the probe strain by a producer (P) kills nearby species that are sensitive to its antibiotic (crossed out S), but is strongly attenuated around an antibiotic-degrading species (right, yellow-green halo around R_d colony). Images are representative of cases without and with three-way interactions among 54 *Streptomyces* pairs tested (1 replica, Extended Data Figs 1 and 2). **c**, Spatial inhibition-zone model. A producer (P) kills nearby species that are sensitive to its antibiotic (crossed out S), but does not affect resistant species (R_i , R_d). Sensitive species are protected by degrader species (right, S within dashed circle around R_d). Surviving species then replicate and disperse over distance $r_{\text{dispersal}}$. **d**, Snapshots of spatial simulations for cyclical three-species, three-antibiotic interaction networks (labels indicate species phenotypes for each antibiotic). **e**, Intrinsically resistant communities collapse with increased dispersal (left), while communities with antibiotic degradation are robust to any level of dispersal (right). Insets show typical sub-region snapshots. Number of species is based on average Shannon diversity of sub-regions (Methods). $r_{\text{dispersal}}$ is measured in grid units (where individual grid cells have side length 1).

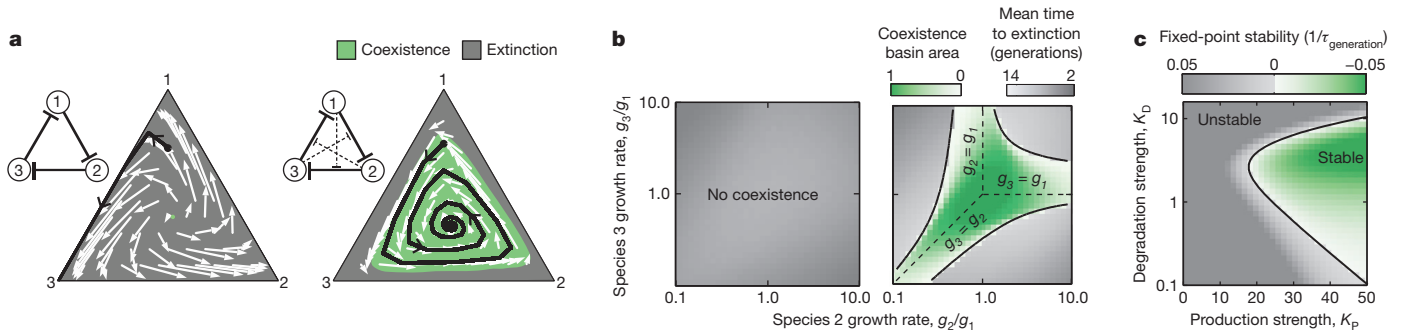


Figure 2 | Strong antibiotic production with intermediate levels of degradation leads to stable communities robust to initial conditions and substantial differences in species growth rates. **a**, Communities with intrinsic resistance diverge from an unstable fixed point (green dot, left), while communities with antibiotic degradation converge towards a stable fixed point within a large basin of attraction (green area, right). Shown in trilinear coordinates are abundance changes per generation (white arrows) and example trajectories (black) for species with inherent growth rates: $g_1 < g_2 < g_3$. **b**, Communities with degradation remain stable even for large differences in

inherent species growth rates (right), while communities with intrinsic resistance are always unstable (left). **c**, Maximal community stability occurs at high levels of antibiotic production (K_p) and intermediate levels of degradation (K_D). Shading shows rate of exponential convergence (green) or escape (grey) from the fixed point. Black lines in panels **b** and **c** show the stability region boundary based on linear stability analysis (Methods). Units for production and degradation strength are species⁻¹; $\tau_{\text{generation}}$ is the number of generations taken to get closer/further to the fixed point by a factor of 10.

ϵ , the only cheater that can invade the community is the production cheater derived from the fastest growing strain (Fig. 3b). This cheater replaces its parent, forming a new community of three species interacting through only two antibiotics. Coexistence in this simpler community is robust to parameter variation (Extended Data Fig. 6) and is also evolutionarily stable: it does not allow invasion by cheaters arising from any of its species (Extended Data Fig. 7). All other cheaters in the

three-species, three-antibiotic community cannot invade, even with a small growth advantage (that is, for small positive ϵ their final abundance is zero; Fig. 3c). With higher growth advantages, these cheaters can ultimately invade by dominating the community, by replacing the parent in a newly formed three-species community, or by generating a new four-species community (Fig. 3c). The emergence of these four-species communities motivated us to search for more complex ecosystems with greater numbers of species and to explore their dynamic behaviours.

Analysis of more complex networks identified many ways for antibiotic production and degradation to generate stability. Randomly sampling larger networks with up to six species and five antibiotics, we found many stable community topologies, all of which included

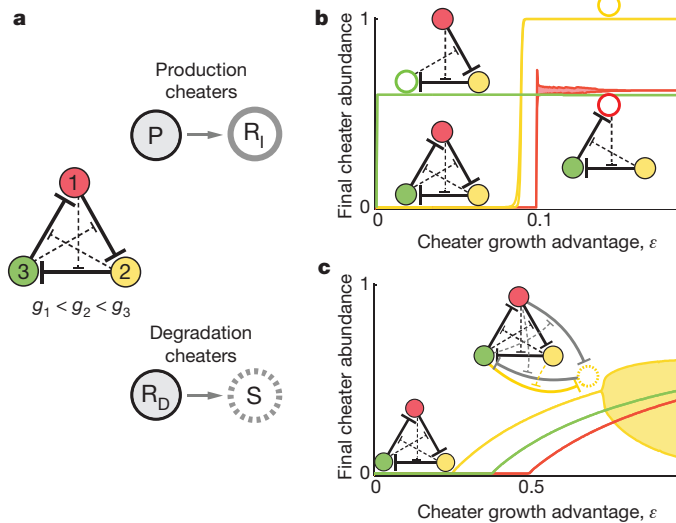


Figure 3 | Communities are robust to invasion by cheaters that cease antibiotic production or degradation. **a**, Production or degradation cheaters (open circles with solid or dashed lines, respectively) are introduced at low abundance into a stable three-species community (filled coloured circles). **b**, When cheater growth advantage ϵ is small, only the production cheater of the fastest growing species can invade (species 3, green). This cheater replaces its parent, forming a new stable community, which is in turn robust to further invasions. The other two production cheaters can invade only when ϵ is large enough, taking over the community (yellow) or replacing their parent in a stable community (red). **c**, Degradation cheaters cannot invade the community at low ϵ , whereas at high enough ϵ they can invade without replacing their parents, rather generating a stable four-species community. A four-species interaction network is shown for the species 2 degradation cheater: grey interactions are inherited from the parent species; yellow interactions are specific to the cheater. Shaded areas span lower/upper bounds when the community exhibits sustained oscillations.

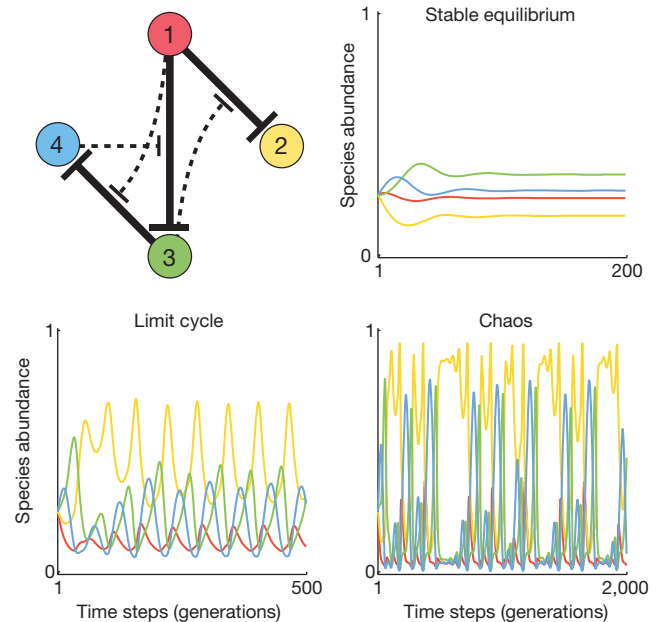


Figure 4 | Complex interaction networks support coexistence through diverse dynamic behaviours. An example of a stable network with four species interacting through production and degradation of three antibiotics. Depending on the strengths of antibiotic production and degradation, this community can coexist through stable equilibrium, limit cycles or chaos (Methods). Line colours indicate species identity.

antibiotic-degrading species (Extended Data Fig. 8). Notably, greater numbers of antibiotics generally increase the number of species that can coexist. While the fraction of network topologies that support stable communities can be small, the combinatorial increase in the number of possible networks provides multitudes of ways for antibiotic production and degradation to generate stable communities with large numbers of species. Coexistence among species in these various network topologies can occur through different dynamic behaviours, including stable fixed points, limit cycles, or chaos, depending on the strengths of antibiotic production K_P and degradation K_D (Fig. 4 and Extended Data Fig. 9). Thus, in addition to enabling the long-term coexistence of complex communities, the combined effect of antibiotic production and degradation can dramatically impact community dynamics.

Our findings suggest new possibilities for engineering multi-species microbial consortia³⁰ and shed light on the role of antibiotic production and degradation in maintaining biodiversity within natural microbial communities. Of course, natural microbial ecosystems are extremely complicated¹³; they contain orders of magnitude more species than we modelled and include additional interactions at the level of resource competition, metabolic cross-feeding, phage invasion, and predator-prey relationships. We expect that further insights into ecosystem stability and assembly will emerge by understanding how these mechanisms generate both pairwise and higher-order multi-species interactions.

Online Content Methods, along with any additional Extended Data display items and Source Data, are available in the online version of the paper; references unique to these sections appear only in the online paper.

Received 26 November 2014; accepted 20 April 2015.

Published online 20 May 2015.

- Hutchinson, G. E. The paradox of the plankton. *Am. Nat.* **95**, 137–145 (1961).
- May, R. M. Will a large complex system be stable? *Nature* **238**, 413–414 (1972).
- Levin, S. A. Dispersion and population interactions. *Am. Nat.* **108**, 207–228 (1974).
- Armstrong, R. A. & McGehee, R. Competitive exclusion. *Am. Nat.* **115**, 151–170 (1980).
- Levin, S. A. Community equilibria and stability, and an extension of the competitive exclusion principle. *Am. Nat.* **104**, 413–423 (1970).
- Stewart, F. M. & Levin, B. R. Partitioning of resources and the outcome of interspecific competition: a model and some general considerations. *Am. Nat.* **107**, 171–198 (1973).
- Levin, B. R. Coexistence of two asexual strains on a single resource. *Science* **175**, 1272–1274 (1972).
- Shoresh, N., Hegreness, M. & Kishony, R. Evolution exacerbates the paradox of the plankton. *Proc. Natl Acad. Sci. USA* **105**, 12365–12369 (2008).
- Durrett, R. & Levin, S. Spatial aspects of interspecific competition. *Theor. Popul. Biol.* **53**, 30–43 (1998).
- Czárán, T. L., Hoekstra, R. F. & Pagie, L. Chemical warfare between microbes promotes biodiversity. *Proc. Natl Acad. Sci. USA* **99**, 786–790 (2002).
- Kerr, B., Riley, M. A., Feldman, M. W. & Bohannan, B. J. M. Local dispersal promotes biodiversity in a real-life game of rock-paper-scissors. *Nature* **418**, 171–174 (2002).
- Reichenbach, T., Mobilia, M. & Frey, E. Mobility promotes and jeopardizes biodiversity in rock-paper-scissors games. *Nature* **448**, 1046–1049 (2007).
- Hibbing, M. E., Fuqua, C., Parsek, M. R. & Peterson, S. B. Bacterial competition: surviving and thriving in the microbial jungle. *Nature Rev. Microbiol.* **8**, 15–25 (2010).
- Chait, R., Vetsigian, K. & Kishony, R. What counters antibiotic resistance in nature? *Nature Chem. Biol.* **8**, 2–5 (2012).
- Conlin, P. L., Chandler, J. R. & Kerr, B. Games of life and death: antibiotic resistance and production through the lens of evolutionary game theory. *Curr. Opin. Microbiol.* **21**, 35–44 (2014).
- Green, J. & Bohannan, B. J. M. Spatial scaling of microbial biodiversity. *Trends Ecol. Evol.* **21**, 501–507 (2006).
- Vetsigian, K., Jajoo, R. & Kishony, R. Structure and evolution of *Streptomyces* interaction networks in soil and in silico. *PLoS Biol.* **9**, e1001184 (2011).
- Cordero, O. X. *et al.* Ecological populations of bacteria act as socially cohesive units of antibiotic production and resistance. *Science* **337**, 1228–1231 (2012).
- Raynaud, X. & Nunan, N. Spatial ecology of bacteria at the microscale in soil. *PLoS ONE* **9**, e87217 (2014).
- Perlin, M. H. *et al.* Protection of *Salmonella* by ampicillin-resistant *Escherichia coli* in the presence of otherwise lethal drug concentrations. *Proc. R. Soc. Lond. B* **276**, 3759–3768 (2009).
- Wright, G. D. Bacterial resistance to antibiotics: enzymatic degradation and modification. *Adv. Drug Deliv. Rev.* **57**, 1451–1470 (2005).
- Wootton, J. T. Indirect effects in complex ecosystems: recent progress and future challenges. *J. Sea Res.* **48**, 1–16 (2002).
- Ohgushi, T., Schmitz, O. & Holt, R. D. *Trait-Mediated Indirect Interactions*. (Cambridge Univ. Press, 2012).
- Bollenbach, T., Quan, S., Chait, R. & Kishony, R. Nonoptimal microbial response to antibiotics underlies suppressive drug interactions. *Cell* **139**, 707–718 (2009).
- Dugatkin, L. A., Perlin, M., Lucas, J. S. & Atlas, R. Group-beneficial traits, frequency-dependent selection and genotypic diversity: an antibiotic resistance paradigm. *Proc. R. Soc. Lond. B* **272**, 79–83 (2005).
- Yurtsev, E. A., Chao, H. X., Datta, M. S., Artemova, T. & Gore, J. Bacterial cheating drives the population dynamics of cooperative antibiotic resistance plasmids. *Mol. Syst. Biol.* **9**, 683 (2013).
- Lenski, R. E. & Hattingh, S. E. Coexistence of two competitors on one resource and one inhibitor: a chemostat model based on bacteria and antibiotics. *J. Theor. Biol.* **122**, 83–93 (1986).
- Hsu, S. B. & Waltman, P. A survey of mathematical models of competition with an inhibitor. *Math. Biosci.* **187**, 53–91 (2004).
- Levin, S. A., Segel, L. A. & Adler, F. R. Diffuse coevolution in plant-herbivore communities. *Theor. Popul. Biol.* **37**, 171–191 (1990).
- Großkopf, T. & Soyer, O. S. Synthetic microbial communities. *Curr. Opin. Microbiol.* **18**, 72–77 (2014).

Supplementary Information is available in the online version of the paper.

Acknowledgements We thank R. Ward, S. Levin, M. Elowitz, G. Bunin, A. Amir, S. Kryazhinskiy, Y. Gerardin, J. Meyer, N. Yin, E. Bairey, H. Chung and A. Palmer for critical feedback and discussions; M. Baym, M. Fischbach, M. Traxler, R. Chait, L. Stone and E. Gontag for strains. E.D.K. acknowledges government support under and awarded by the Department of Defense, Office of Naval Research, National Defense Science and Engineering Graduate (NDSEG) Fellowship, 32 CFR 168a. J.Z. acknowledges support from the Research Science Institute at MIT during the summer of 2011. K.V. acknowledges start-up funds from University of Wisconsin-Madison. R.K. acknowledges the support of a James S. McDonnell Foundation 21st Century Science Initiative in Studying Complex Systems Research Award 220020169, National Institutes of Health Grant R01GM081617, European Research Council Seventh Framework Programme ERC Grant 281891, Israeli Centers of Research Excellence I-CORE Program ISF Grant No. 152/11.

Author Contributions E.D.K., K.V. and R.K. designed the study; E.D.K., K.V. and J.Z. did the experiments; E.D.K. and K.V. did the simulations and modelling; E.D.K., K.V. and R.K. analysed the data and wrote the paper.

Author Information Reprints and permissions information is available at www.nature.com/reprints. The authors declare no competing financial interests. Readers are welcome to comment on the online version of the paper. Correspondence and requests for materials should be addressed to K.V. (kalin@discovery.wisc.edu) and R.K. (rkishony@technion.ac.il).

METHODS

Mixed inhibition-zone model of cyclic three-species communities. *Model description.* We derived a formula for the changes of species abundances in the inhibition-zone model for the limit of complete mixing after each time step ($r_{\text{dispersal}} \rightarrow \infty$) and infinite population size. Let X_i be the abundance of species i per unit area, K_P the killing area around each producer and K_D the degradation area around each degrader. Since species disperse randomly, the fitness f_i of species i depends on its inherent growth rate g_i and the fraction of area $1 - P_{\text{kill}}$ in which it is not killed by antibiotics:

$$f_i = g_i(1 - P_{\text{kill}}).$$

For each antibiotic, a sensitive individual S will only be killed if it is located where there is at least one producer P within a K_P neighbourhood and there is no protecting antibiotic-degrading (R_D) species within a K_D neighbourhood. Since individuals are randomly placed, the number of cells within such neighbourhoods follows a Poisson distribution, so that if λ is the expected number of cells in a region then the probability of having zero cells in the region is $e^{-\lambda}$. Thus the probability of being in the killing zone of the producer is $1 - e^{-K_P X_P}$, and the probability of not being in the degradation zone of R_D is $e^{-K_D X_D}$, where X_P and X_D are respectively the abundances of species producing and degrading the antibiotic. Combining these we obtain

$$P_{\text{kill}} = e^{-K_D X_D} (1 - e^{-K_P X_P})$$

Thus for the cyclic three-species network the fitness of each species is:

$$f_1 = g_1 (1 - e^{-K_D X_2} (1 - e^{-K_P X_3}))$$

$$f_2 = g_2 (1 - e^{-K_D X_3} (1 - e^{-K_P X_1}))$$

$$f_3 = g_3 (1 - e^{-K_D X_1} (1 - e^{-K_P X_2}))$$

We update species abundance for each time step using the discrete time formula:

$$X_i(t+1) = \frac{X_i(t)f_i(t)}{\sum_j X_j(t)f_j(t)}$$

where the denominator ensures that total species abundance remains constant. *Linear stability analysis.* We found the fixed point numerically for each set of parameters and then found the eigenvalues of the Jacobian computed at the fixed point. The logarithm of the maximum absolute value of the eigenvalues was used as a stability measure in Fig. 2b, c to determine the region of stability. The fixed point is stable if this value is less than zero.

Robustness to mutation and invasion by cheating species. Each cheating species was cloned from a parent by copying all antibiotic phenotypes except for a mutation in the phenotype with respect to a single antibiotic: $P \rightarrow R_1$ for production cheaters, and $R_D \rightarrow S$ for degradation cheaters. Starting with a three-species community at equilibrium, we added a small amount of the cheating species ($X_{\text{cheater}} = 0.001$, with abundances of the other species renormalized so that $\sum X_i = 1$). We set the growth rate of the cheater to the parental growth rate with a growth advantage ε , so that $g_{\text{cheater}} = (1 + \varepsilon)g_{\text{parent}}$. We ran each simulation until species abundances reached steady state or stable oscillations, and then we calculated the minimum and maximum values for each cheater during the last third of the simulation time.

Coexistence of communities with three species and two antibiotics. Cyclic three-species communities maintain coexistence even when the fastest growing species ceases antibiotic production, resulting in a simpler three-species, two-antibiotic community. This network exhibits robust coexistence similar to the three-antibiotic network, so long as the species that does not produce antibiotics is the fastest growing species (Extended Data Fig. 6a). This simpler community also resists invasion by any remaining production or degradation cheaters (Extended Data Fig. 7b).

We investigated whether further reductions of this network support coexistence. While coexistence is possible when only one of the two antibiotics is degraded, this coexistence occurs only for a small range of parameter values (Extended Data Fig. 6b). Based on a comprehensive sampling of parameter space, we found that further reductions to communities that produce only a single antibiotic do not support coexistence when inherent growth rates differ. This is consistent with the intuition that when only one antibiotic is being produced there will always be two species that are equivalent with respect to the antibiotic, which will lead to extinction of the slower-growing species. Thus, in contrast to spatial models where coexistence is possible on a single antibiotic¹¹, coexistence in well-mixed models requires three species and at least two antibiotics.

Generalizing the mixed inhibition-zone model for arbitrary interaction networks. *Model description.* We calculated the probability of each species being inhibited for a general ecosystem with n_s species and n_a antibiotics, where species

can be any of the four antibiotic phenotypes (P, S, R_1 or R_D) for each antibiotic. The assumptions are the same as for the mixed inhibition-zone model of cyclic three-species communities. Consider the situation in which antibiotic production is stronger than degradation ($K_P > K_D$, the other scenario follows similarly). For an individual of a target sensitive species, each of the other $n_s - 1$ species can be either near enough to affect the target through production and degradation of some of the antibiotics (with probability P_{near}), can be at intermediate distances in which they affect the target through production but not degradation ($P_{\text{intermediate}}$), or can be far away so that they do not affect the target in any way (P_{far}). These three distance ranges make for $3^{n_s - 1}$ possible combinations for the presence or absence of the other species within any neighbourhood of the target species. Based on the phenotypes of the sensitive target species and the other species, we calculated all combinations that result in antibiotic inhibition. For each species i , we calculated the probabilities P_{near} , $P_{\text{intermediate}}$ and P_{far} from the levels of production and degradation of the antibiotics, in this case:

$$P_{\text{near}} = 1 - e^{-K_D X_i}$$

$$P_{\text{far}} = e^{-K_P X_i}$$

$$P_{\text{intermediate}} = P_{\text{far}} - P_{\text{near}}$$

Combining these, we calculated the probability P_c of each inhibitory combination occurring, multiplying the probabilities of each species being either near, intermediate, or far according to the requirements of each combination. Finally, we obtained the total probability of the target species being inhibited by summing across all possible inhibitory combinations with $P_{\text{kill}} = \sum_c P_c$. As in the three-species model we let the fitness of each species be:

$$f_i = g_i(1 - P_{\text{kill}})$$

and

$$X_i(t+1) = \frac{X_i(t)f_i(t)}{\sum_j X_j(t)f_j(t)}$$

Testing for coexistence in more complex networks. We randomly sampled up to 10^6 networks for each combination of 4–6 initial species and 1–5 initial antibiotics by randomly choosing one of the four phenotypes (S, P, R_1 or R_D) for each species/antibiotic combination. When the total number of possible networks was less than 10^6 we tested all networks. We excluded networks that contained antibiotics or species with identical properties from subsequent simulations, since these are equivalent to instances of networks with a smaller number of antibiotics or species. With n_a initial antibiotics and n_s initial species at initial abundances $1/n_s$, we calculated the number of final species surviving at abundance $X_i > 0.01/n_s$ after 10,000 time steps. Simulations were binned by the maximum number of surviving species across all possible combinations of the parameters: $g_{\text{max}} = (1.2 \text{ or } 2.5)$, $K_P = (10 \text{ or } 30)$ and $K_D = (3 \text{ or } 10)$. For a given g_{max} , species growth rates were evenly spaced between 1.0 and g_{max} . With total number of network topologies $n_{\text{total}} = 4^{n_s n_a} / n_a!$, even this sparse sampling of parameters shows that the total number of topologies that support stability is quite large (Extended Data Fig. 8).

Calculating effective number of species using Shannon diversity. We calculated effective species numbers by the Shannon entropy H of the species distribution:

$$H = - \sum_i X_i \log_2 X_i$$

with species frequencies X_i normalized such that $\sum_i X_i = 1$. Effective number of species is then given by 2^H .

Chemostat model of cyclic three-species communities. *Model description.* Our chemostat model is adapted from classical models of antibiotic interactions with a constant inflow of a single resource and constant dilution²⁸. Ordinary differential equations track the concentration of the resource (Z), the abundances of three species (X_i), and the concentrations of three antibiotics (C_i), implementing the cyclical interaction network as described previously. Each species consumes resources and produce antibiotics. The species degrade antibiotics to which they are resistant, and their growth is inhibited by antibiotics to which they are sensitive. The resource dynamic is:

$$\frac{dZ}{dt} = (Z_0 - Z)D - \sum_i \frac{X_i G_i}{m},$$

where Z_0 is the concentration of the added resource, D is the dilution rate, G_i a function that describes the growth rate of species i considering antibiotic and resource levels, and m is a conversion factor between resources and species,

so that G_i/m is the resource consumption rate of each species. The species abundances change according to:

$$\frac{dX_i}{dt} = X_i(G_i - D) \text{ with } G_i = g_i \frac{Z}{k_z + Z} e^{-K_p C_j}.$$

Growth rate increases with the concentration of resources following Monod kinetics, where k_z determines the concentration of half-maximal resource absorption. The growth rate is also affected by antibiotics, decreasing exponentially with the level of antibiotics to which a species is sensitive (here an antibiotic with concentration C_j inhibits species i). The parameter K_p characterizes the strength of antibiotic inhibition, and g_i is a species-specific maximal growth rate.

The antibiotic concentration dynamics are given by:

$$\frac{dC_j}{dt} = pX_jG_j - K_D X_k C_j - DC_j$$

The parameter p determines the amount of antibiotics produced per cell division, the second term assumes that species k degrades the antibiotic produced by species j through mass action kinetics, and the parameter K_D characterizes the strength of antibiotic degradation.

Rescaled chemostat model. To analyze the stability of the three-species three-antibiotic interaction network, we first note that

$$\frac{d}{dt} \left(\sum_i \frac{X_i}{m} - Z_o + Z \right) = -D \left(\sum_i \frac{X_i}{m} - Z_o + Z \right),$$

and therefore after a transient

$$Z = Z_o - \sum_i X_i / m$$

which allows us to eliminate the resource concentration degree of freedom.

We rescale variables to reduce the number of free parameters: time so that $D = 1$, Z and k_z so that $Z_o = 1$, and we eliminate m by substituting $X_i' = X_i/m$, $C_i' = C_i/m$, $K_p' = mK_p$ and $K_D' = mK_D$. Dropping the primes we obtain:

$$\frac{dX_i}{dt} = X_i(G_i - 1)$$

$$G_i = g_i \frac{1 - \sum_j X_j}{k_z + 1 - \sum_j X_j} e^{-K_p C_j}$$

$$\frac{dC_j}{dt} = pX_jG_j - K_D X_k C_j - C_j$$

Linear stability analysis. The problem of finding the fixed point in the rescaled model was reduced to a single nonlinear algebraic equation, which was numerically solved for different parameters to determine the corresponding equilibria for X_i and C_j . At the fixed point $\frac{dX_i}{dt} = 0$, and therefore $G_i = 1$. This allows us to express the C_j variables as functions of

$$\Theta = \frac{1 - \sum_i X_i}{k_z + 1 - \sum_i X_i}$$

and the g_i constants. Substituting the expressions for C_j into

$$pX_jG_j - K_D X_k C_j - C_j = 0$$

results in a system of linear equations for X_i terms, which can be solved as a function of Θ . This allows us to express $\sum_i X_i$ as a function of Θ and thus obtain a nonlinear equation for Θ . For Extended Data Fig. 5a, the stability of the fixed point was determined by finding the eigenvalues of the Jacobian at the fixed point. A negative largest real component of the eigenvalues indicates stability.

Parameter values for main text figures. Fig. 1: grids were 200×200 with wrapping boundaries. Species were initially randomly seeded on the grid at low total abundance (1%), or in an initial configuration with three large domains for $r_{\text{dispersal}} > 20$ to reduce the initial chance of extinction of all species at high levels of mixing (with intrinsic resistance). Fig. 1e, lines show average of ten simulations, calculating the effective species numbers based on Shannon diversity of species within 40×40 sub-regions (shown in insets) at 100 evenly spaced locations on the grid at the final time; other parameters: $r_{\text{production}} = 3$, $r_{\text{degradation}} = 3$, $r_{\text{dispersal}} = (3, 4, 6, 10, 20, 80, 200)$; runtimes for each $r_{\text{dispersal}}$ are respectively: (150, 150, 75, 75, 75, 25, 25), after which the overall spatial patterns were relatively unchanging. For intrinsic resistance with $r_{\text{dispersal}} = (80, 200)$ it was possible for all species to be inhibited at the same time step, in which case we chose one cell at random to proceed to the next generation.

Fig. 2: we estimated the size of the basin of attraction by running simulations starting from 210 different initial species abundances that were equally spaced on a triangle lattice inside the $x_1 + x_2 + x_3 = 1$ two-dimensional simplex. The basin of attraction area is the fraction of simulations that move to the fixed point with all three species coexisting. Fig. 2a, $g_1 = 1.0$, $g_2 = 1.1$, $g_3 = 1.2$; left: $K_p = 4$, $K_D = 0$;

right: $K_p = 12$, $K_D = 3$. Fig. 2b, left: $K_p = 4$, $K_D = 0$; right: $K_p = 40$, $K_D = 4$. Fig. 2c, $g_1 = 1$, $g_2 = 3$, $g_3 = 2$.

Fig. 3: $g_1 = 1.0$, $g_2 = 1.1$, $g_3 = 1.2$, $K_p = 16$, $K_D = 4$.

Fig. 4: $g_1 = 1.0$, $g_2 = 1 + 1/30$, $g_3 = 1 + 2/30$, $g_4 = 1.1$; stable equilibrium: $K_p = 10$, $K_D = 10$; limit cycles: $K_p = 12$, $K_D = 20$; chaos: $K_p = 20$, $K_D = 55$.

Code availability. MATLAB code for the spatial inhibition-zone model, mixed inhibition-zone model and chemostat model is available from the authors upon request.

Note on the mechanism of three-way attenuating interactions. Antibiotic degradation is a common mechanism of antibiotic resistance²¹ and is therefore a probable mechanism for the attenuation of inhibition that we observed in the three-species interaction assays and the antibiotic modulation assays (Extended Data Figs 1 and 2). There is strong evidence in support of this assumption based on many reports of antibiotic degrading species protecting sensitive species from antibiotics^{20,25,26,31–33}. Antibiotic degradation is also a known mechanism of resistance for the antibiotics in which we observed significant attenuation (Extended Data Fig. 1c): tobramycin³⁴, ciprofloxacin³⁵, β -lactam antibiotics³⁶ (cefotaxime, piperacillin, penicillin), nitrofurantoin³⁷, rifampin³⁸ and trimethoprim³². Furthermore, we experimentally confirmed that degradation through β -lactamases contributes to the attenuation of β -lactam antibiotics through a modified version of the antibiotic modulation assays that uses β -lactamase inhibitors (Extended Data Figs 1d and 2c). However, we note that the models we use can be easily generalized to additional mechanisms that generate antibiotic attenuation, for example through antibiotic suppression^{24,39}.

Interaction experiments. No statistical methods were used to predetermine sample size. **Three-species interaction assays.** All possible pairings of 16 *Streptomyces* species from a spore collection (~ 100 spores per μl) were pinned 1 cm apart on 9-cm Petri dishes with $1 \times$ oatmeal agar, and plates were grown in a darkened plastic bin for 13 days at room temperature. Overlay media without thiamine was prepared in test tubes in 5-ml aliquots, melted in an autoclave (to melt, not sterilize), and cooled to 42°C in a water bath. An overnight liquid-broth culture of *E. coli* expressing YFP was mixed 9:1 with $1,000 \times$ thiamine stock, $50 \mu\text{l}$ of the *E. coli* mixture was added to overlay agar, quickly vortexed to mix and then poured uniformly onto the plate. Plates were incubated at 37°C for 18 h and photographed in bright field and YFP channels to record the antibiotic inhibition zone. Combinations in which one species created a large inhibition zone were scored using the modulation index $M = (r_m - r_o)/(r_m + r_o)$, where r_m is the radius of the inhibition zone in the direction of the modulator and r_o is the radius of the inhibition zone in the opposite direction. Extended Data Fig. 1b shows data from 54 combinations in which one species made a large inhibition zone, with five antibiotic producers and 11 modulator species (one plate removed due to contamination). Extended Data Fig. 2a shows images and scoring. We observed similar attenuation in follow-up technical replicas of individual strain combinations and when testing on other media.

Antibiotic modulation assays. Antibiotic modulation assays were similar to the three-species assays except that the antibiotic producing species was replaced with pure antibiotic and the assay geometry was modified to enable more high-throughput measurements. Modulator inoculation plates were prepared by spreading $50 \mu\text{l}$ of 20% glycerol spore stocks onto $1/2 \times$ oatmeal agar 9-cm Petri dishes with glass beads, incubated for 1 week at 30°C in plastic bins, then stored at room temperature. 25 ml of $1/2 \times$ oatmeal agar was spread evenly over a 14-cm Petri dish. On day 1, a small amount of antibiotic stock was pipetted onto the centre of the agar, absorbed and stored at 30°C (cefotaxime $10 \mu\text{l}$, chloramphenicol $10 \mu\text{l}$, ciprofloxacin $10 \mu\text{l}$, doxycycline $10 \mu\text{l}$, nitrofurantoin $20 \mu\text{l}$, penicillin $20 \mu\text{l}$, piperacillin $15 \mu\text{l}$, rifampicin $20 \mu\text{l}$, tobramycin $40 \mu\text{l}$, trimethoprim $20 \mu\text{l}$). On day 2, a thin radial line for each of three modulator species was inoculated using the edges of sterilized 60-mm cover glass (VWR 48393-070) onto the 14-cm Petri dish. Plates were incubated in plastic bins at 30°C for 3 days and small areas of contamination were cut out of the agar. Overlay media was prepared in 25-ml aliquots, as in the three-species assays. Overnight cultures of yellow fluorescent protein (YFP) and cyan fluorescent protein (CFP) producing *E. coli* were combined at equal ratios (by OD) and mixed 9:1 with $1,000 \times$ thiamine stock. 1 ml of the *E. coli* mixture was added to the overlay media, vortexed, and poured evenly over the surface of the oatmeal agar. All plates were incubated at 37°C between 16–21 h and photographed in bright field, YFP and CFP channels to record the antibiotic inhibition zone. Test strains included the two strongest attenuators from the three-species assay, *Streptomyces coelicolor* and a collection of soil isolates from Massachusetts and Colorado soils. Combinations were marked with a dot for significance in Extended Data Fig. 1c where the average modulation index M deviated from 0 by at least twice the standard error in the mean ($P < 0.05$, two-sided t -test, $n = 3$ technical replicas). These images were also visually inspected to confirm warping of the inhibition-zone boundary. Extended Data Fig. 2b shows examples and scoring for different antibiotics.

β -Lactamase inhibitor assays. 1 ml of 1 mM β -lactamase inhibitor was spread evenly over 14-cm 1/2 \times oatmeal plates with glass beads and allowed to dry in a ventilation hood (to minimize contamination). Overlay with YFP and CFP *E. coli* was the same as the antibiotic modulation assay except that 1 ml of 1 mM β -lactamase inhibitor stock was added to the overlay media and vortexed before adding *E. coli*. Extended Data Fig. 1d shows data for a collection of 14 species, four antibiotics and three β -lactamase inhibitors. Extended Data Fig. 2c shows example assay images.

Isolation of soil bacteria. Isolation and identification of five *Streptomyces* from soil A (Massachusetts) as described in ref. 17. We chose five strains from a collection of 47 isolates that did not produce strong antibiotic inhibition zones on oatmeal agar. Soil B (Colorado) was collected from White River National Forest in unincorporated Pitkin County. We chose ten strains from a collection of 55 isolates that did not produce strong inhibition zones, including two *Streptomyces* species, five Actinobacteria species and three non-Actinobacteria species. Species identification was through Sanger sequencing of 16S ribosomal DNA.

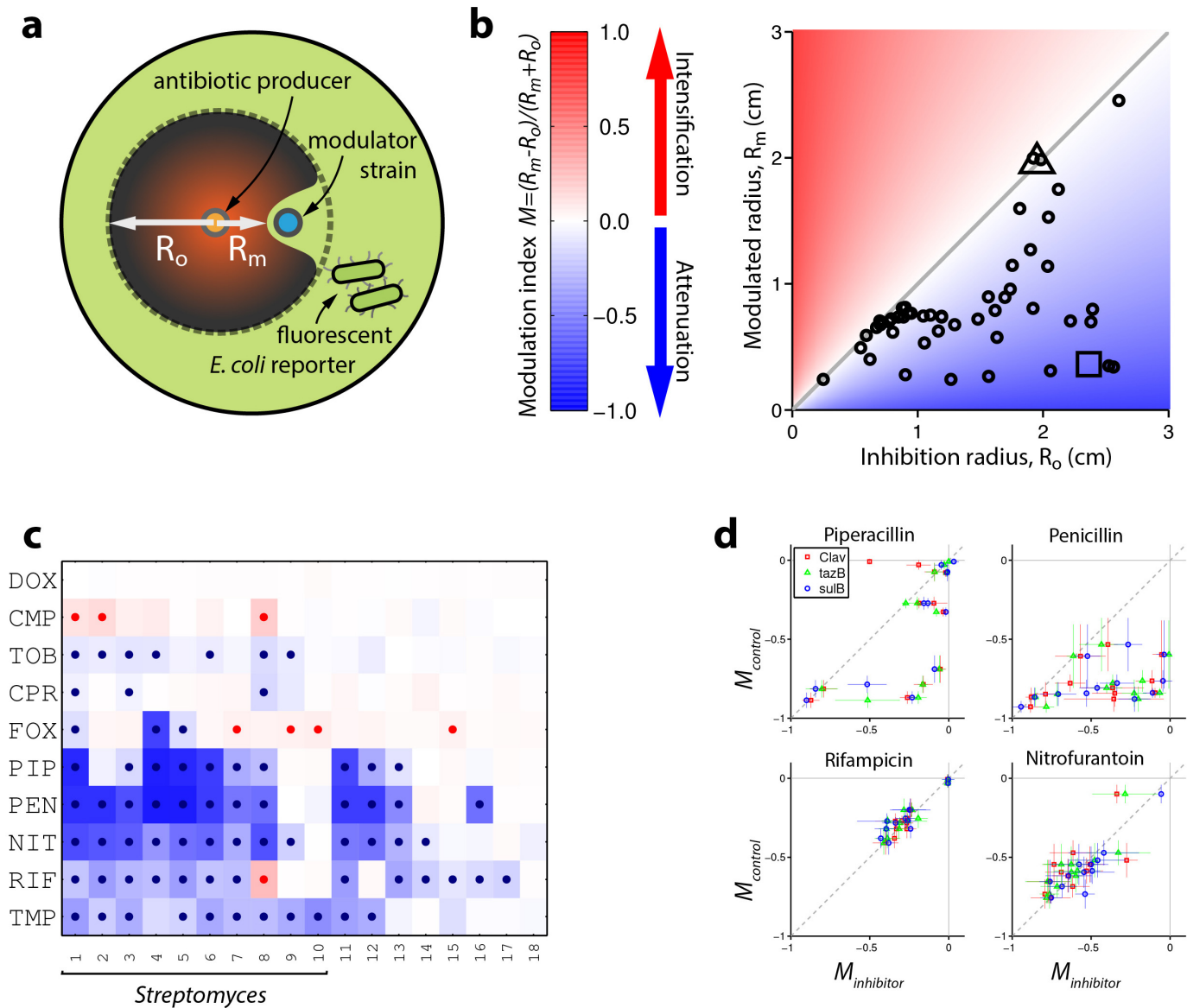
Imaging and data analysis. The three-species assay images were photographed using a custom-built automated fluorescent imaging system as described in ref. 40. Other assays were using a similar but newer system. Levels of antibiotic modulation were scored by manually recording the edges of the inhibition zones of the fluorescent *E. coli* using MATLAB. Example images were normalized to fill the dynamic range and gamma adjusted to improve contrast.

Growth media. 1 \times oatmeal agar: 72.5 g l⁻¹ Difco oatmeal agar (BD). 1/2 \times oatmeal agar: 31.25 g l⁻¹ Difco oatmeal agar (BD) and 6.25 g l⁻¹ Bacto agar (BD), with \sim 100 μ l l⁻¹ 10 M NaOH to adjust to pH 7. Media for overlays consisted of M63 salts (2 g l⁻¹ (NH₄)₂SO₄, 13.6 g l⁻¹ KH₂PO₄, 0.5 mg l⁻¹ FeSO₄7H₂O) supplemented with 0.4% glucose, 0.02% casamino acids, 1 mM MgSO₄, 1.5 mM thiamine, 7.5 g l⁻¹ bacto-agar (BD), adjusting pH to 7.0 with 1 M NaOH. 1,000 \times thiamine was prepared at 1.5 M in H₂O and filter sterilized.

Chemical stocks. Cefoxitin (Sigma C-4786) 50 mg ml⁻¹ in H₂O, chloramphenicol (Sigma C0378) 30 mg ml⁻¹ in EtOH, ciprofloxacin (Sigma 17850) 10 mg ml⁻¹ in

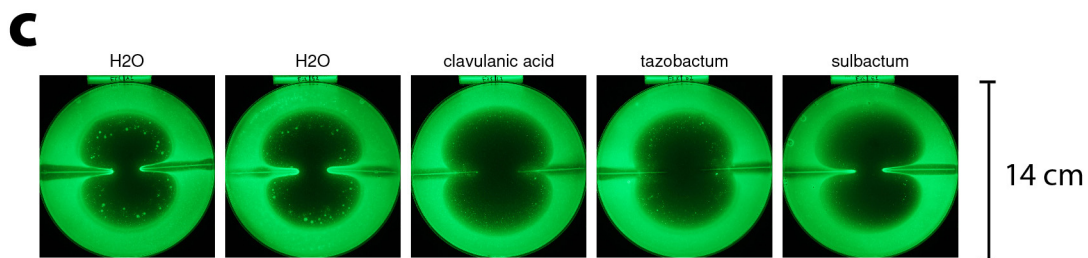
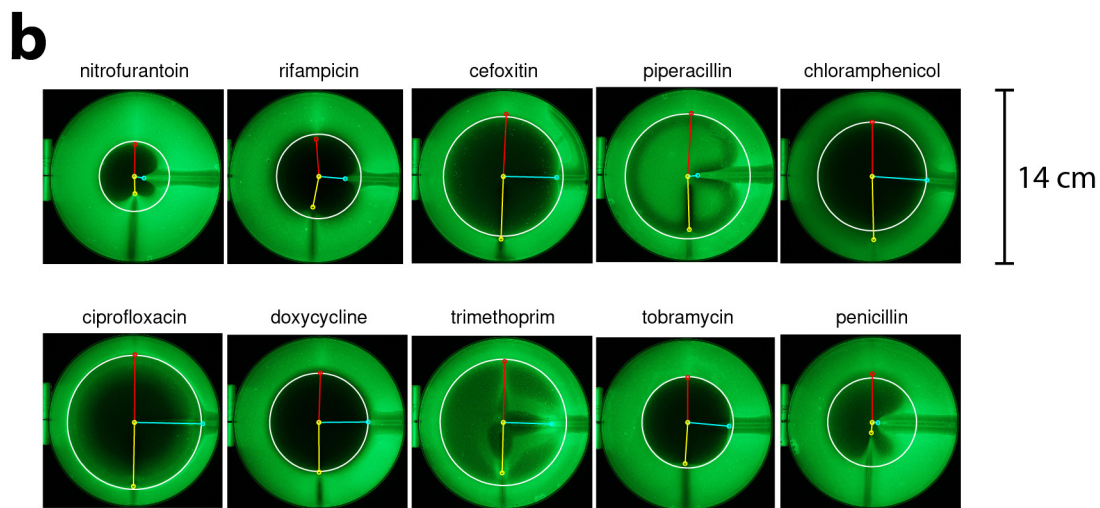
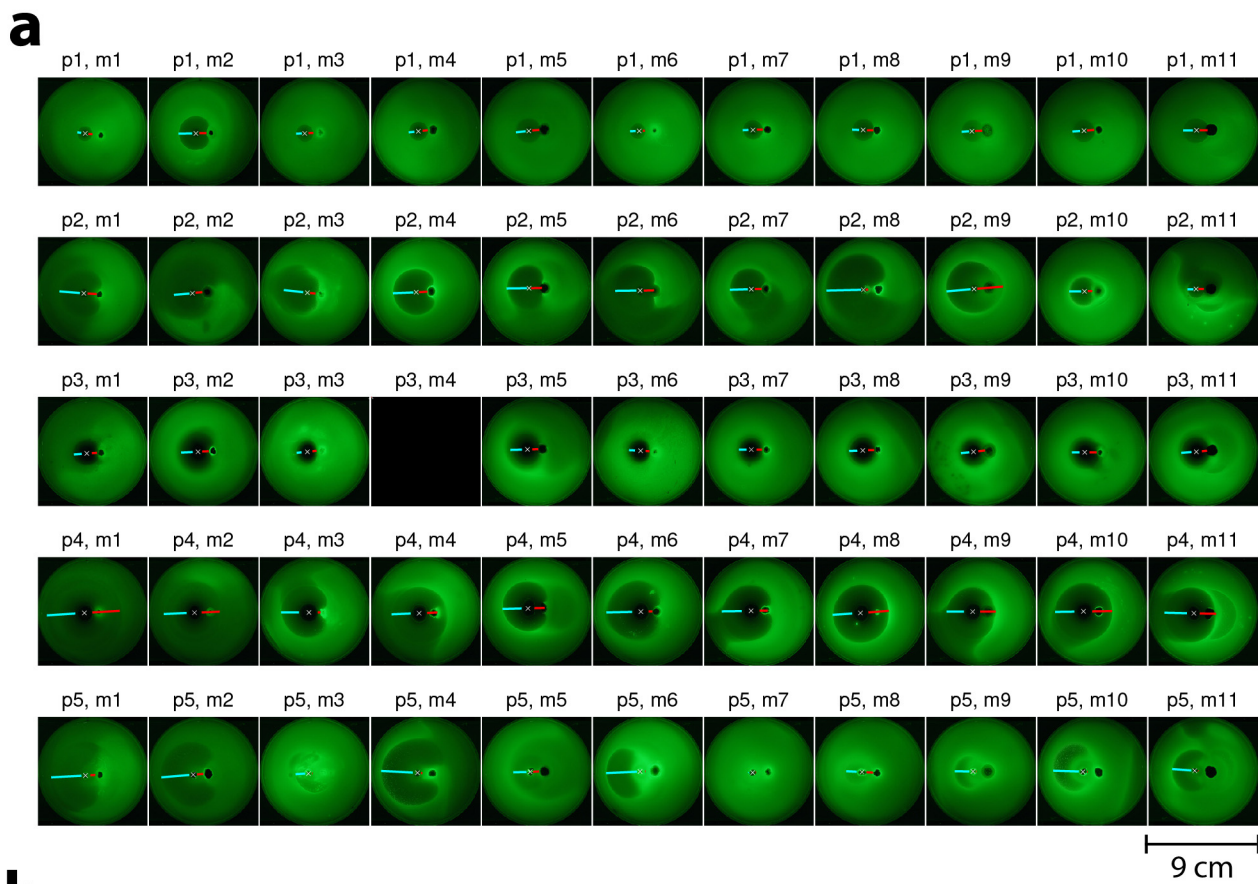
H₂O + 3 μ l ml⁻¹ 10 M HCl, doxycyclin (Sigma D-9891) 50 mg ml⁻¹ in H₂O, nitrofurantoin (Sigma N7878) 10 mg ml⁻¹ in DMF, penicillin (Sigma 13750) 50 mg ml⁻¹ in H₂O, piperacillin (Sigma P8396) 50 mg ml⁻¹ in H₂O, rifampicin (Sigma R3501) 16 mg ml⁻¹ in DMSO, tobramycin (Sigma T4014) 50 mg ml⁻¹ in H₂O, and trimethoprim (Sigma T7883) 5 mg ml⁻¹ in H₂O. β -Lactamase inhibitors were prepared at 1 mM in H₂O: clavulanic acid (as potassium clavulanate, Sigma 33454), tazobactam sodium salt (Sigma T2820), sulbactam (Sigma S9701).

31. D'Costa, V. M. Sampling the antibiotic resistome. *Science* **311**, 374–377 (2006).
32. Walsh, F. & Duffy, B. The culturable soil antibiotic resistome: a community of multi-drug resistant bacteria. *PLoS ONE* **8**, e65567 (2013).
33. Brook, I. The role of beta-lactamase-producing-bacteria in mixed infections. *BMC Infect. Dis.* **9**, 202 (2009).
34. Shaw, K. J., Rather, P. N., Hare, R. S. & Miller, G. H. Molecular genetics of aminoglycoside resistance genes and familial relationships of the aminoglycoside-modifying enzymes. *Microbiol. Rev.* **57**, 138–163 (1993).
35. Wetzstein, H. G., Stadler, M., Tichy, H. V., Dalhoff, A. & Karl, W. Degradation of ciprofloxacin by basidiomycetes and identification of metabolites generated by the brown rot fungus *Gloeophyllum striatum*. *Appl. Environ. Microbiol.* **65**, 1556–1563 (1999).
36. Livermore, D. M. β -Lactamases in laboratory and clinical resistance. *Clin. Microbiol. Rev.* **8**, 557–584 (1995).
37. Rafii, F. & Hansen, E. B. Isolation of nitrofurantoin-resistant mutants of nitroreductase-producing *Clostridium* sp. strains from the human intestinal tract. *Antimicrob. Agents Chemother.* **42**, 1121–1126 (1998).
38. Hoshino, Y. *et al.* Monoxygenation of rifampicin catalyzed by the rox gene product of *Nocardia farcinica*: structure elucidation, gene identification and role in drug resistance. *J. Antibiot. (Tokyo)* **63**, 23–28 (2010).
39. Chait, R., Craney, A. & Kishony, R. Antibiotic interactions that select against resistance. *Nature* **446**, 668–671 (2007).
40. Chait, R., Shrestha, S., Shah, A. K., Michel, J.-B. & Kishony, R. A differential drug screen for compounds that select against antibiotic resistance. *PLoS ONE* **5**, e15179 (2010).



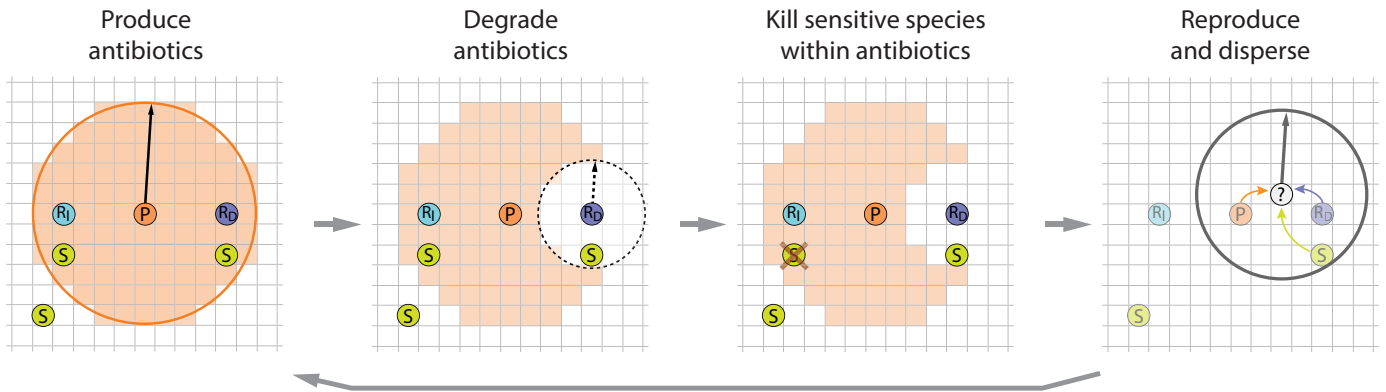
Extended Data Figure 1 | Antibiotic attenuation is widespread among natural antibiotic producing species isolated from soil. **a**, Diagram of three-species assays: measuring the antibiotic inhibition zone of *E. coli* around a producer strain enables quantification of three-species interactions caused by a modulator strain. **b**, Attenuating interactions dominate among a set of 54 *Streptomyces* producer-modulator combinations. Triangle and square markers show scoring from example images in Fig. 1b, left and right respectively. **c**, Antibiotic modulation assays: attenuating interactions dominate among combinations of soil species with a panel of ten pure antibiotics. Combinations are coloured by modulation index as in **b** and marked with a dot where the modulation index is significantly different from zero ($n = 3$, Methods). Strains 1 and 2 are the strongest modulators from the three-species assays, strain three is

Streptomyces coelicolor, strains 4–18 are additional soil isolates (Extended Data Table 1). DOX, doxycycline; CMP, chloramphenicol; TOB, tobramycin; CPR, ciprofloxacin; FOX, cefoxitin; PIP, piperacillin; PEN, penicillin; NIT, nitrofurantoin; RIF, rifampicin; TMP, trimethoprim. **d**, Scatter plots of average modulation index M for 12 species from panel **c**, with and without β -lactamase inhibitors. Points occur off the diagonal for the β -lactams piperacillin and penicillin but near the diagonal for the structurally unrelated antibiotics rifampin and nitrofurantoin, consistent with attenuation of the β -lactams through a mechanism of antibiotic degradation. Error bars are standard error of the mean for technical replicas with inhibitor ($n = 3$) or without inhibitor (control, $n = 6$). Control is addition of H_2O instead of inhibitor. Clav, clavulanic acid; tazB, tazobactam; sulB, sulbactam.



Extended Data Figure 2 | Example images from three-species interaction assays and antibiotic assays. **a**, Images and scoring for three-species interaction assays from Extended Data Fig. 1b. p indicates producer species, m indicates potential modulator species. **b**, Example images and scoring from the antibiotic modulation assays from Extended Data Fig. 1c. Each plate shows tests for modulation of antibiotic inhibition for three different species against a different antibiotic. Colour lines show the size of the inhibition zone at the

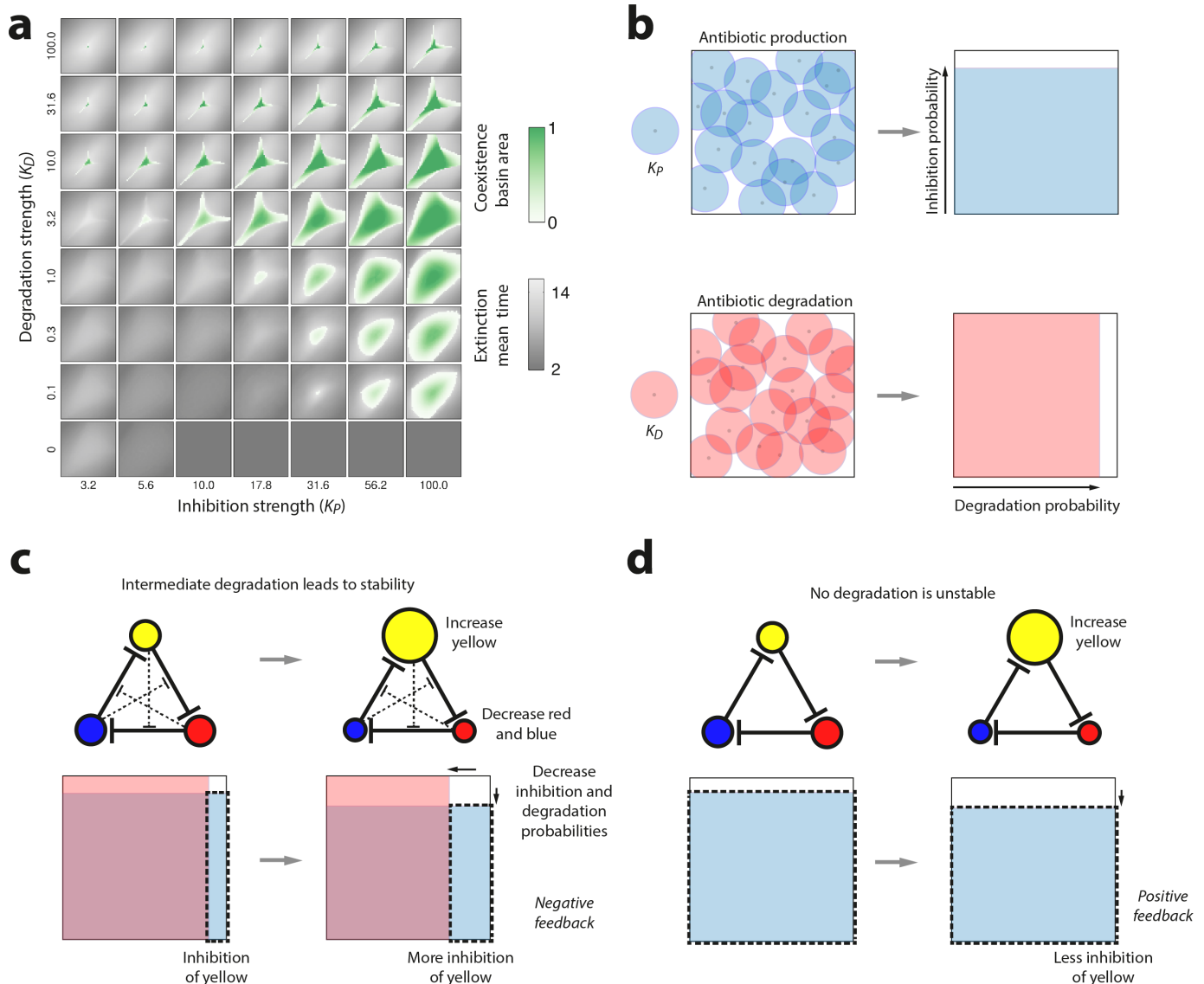
location of the radially positioned modulator species; the white circles show the radius of the zone of inhibition as inferred from the left side of the plate that contains no modulators. **c**, Example images from an antibiotic modulation assay with β -lactamase inhibitors and the β -lactam antibiotic cefoxitin. Left and right side of each plate is inoculated with a line of species four from Extended Data Fig. 1c. Attenuation is significantly reduced by the β -lactamase inhibitors (especially clavulanic acid and tazobactam) when compared to controls (H_2O).



Extended Data Figure 3 | Illustration of the spatial inhibition-zone model.

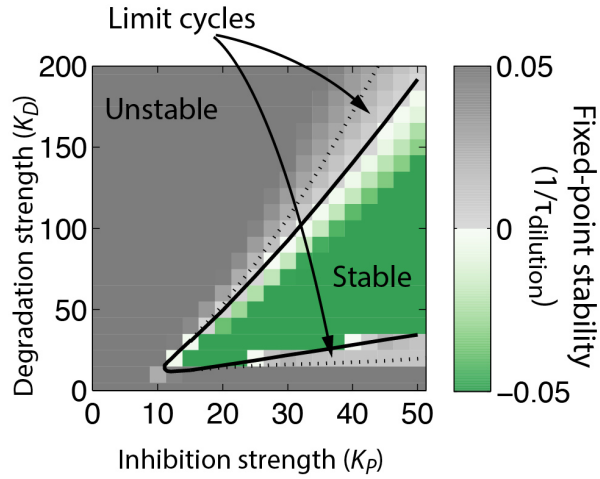
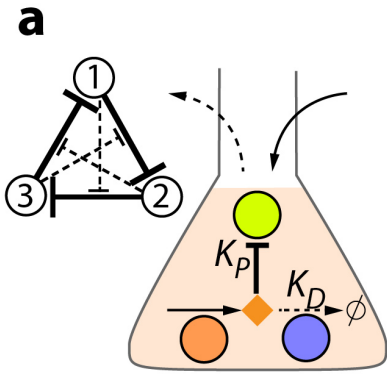
The simulation is performed on a grid of size $L \times L$. A single individual occupies each grid location. During each generation: (1) Individuals from species of type P produce antibiotics within a circle of radius $r_{\text{production}}$; (2) individuals of type R_D remove antibiotics within a circle of radius $r_{\text{degradation}}$. This process is repeated for each of the different antibiotics; (3) all sensitive

individuals (type S) are killed at any locations that still contain the corresponding antibiotics (crossed out S; antibiotic values at each location are calculated at centre positions); (4) empty locations of a new grid are filled by randomly choosing from any surviving individuals within a radius $r_{\text{dispersal}}$. If there are no surviving individuals within $r_{\text{dispersal}}$ then an empty location remains empty.

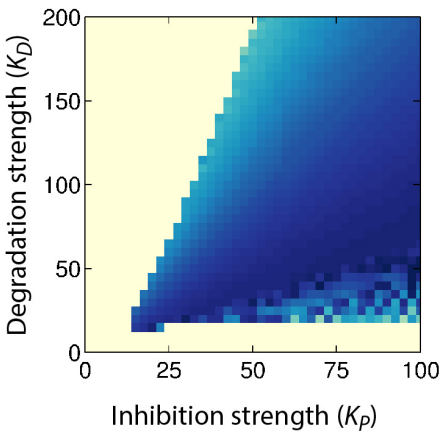


Extended Data Figure 4 | Dependence of coexistence on degradation in the mixed inhibition-zone model. **a**, Stability analysis of the full parameter space in the mixed inhibition-zone model. Using simulations, we tested the stability of cyclic three-species, three-antibiotic communities with dense sampling of all possible parameters for the inhibition-zone model, varying strengths of production (K_P) and degradation (K_D), initial abundances of species 1–3 and growth ratios g_2/g_1 and g_3/g_1 . As in Fig. 2b, each grid shows a 100-fold range of growth rate ratios from 0.1 to 10. Large basins of attraction exist across a wide range of parameter values, with maximal stability at high levels of antibiotic production and intermediate levels of degradation. **b–d**, Intuition for why coexistence depends on degradation. **b**, The inhibition-zone model calculates the probability of a given sensitive

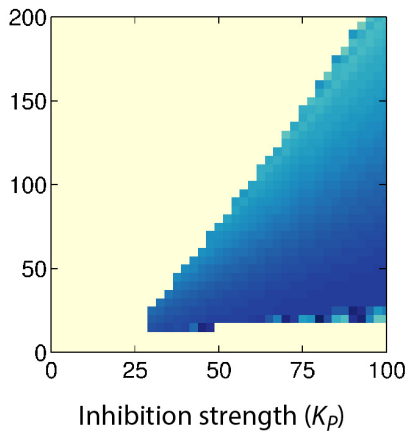
species being inhibited by an antibiotic producer (blue), or being protected by a degrading species (red), given the relative strengths of production (K_P) and degradation (K_D). The expected area covered by the overlapping circles (left) is used to calculate the corresponding inhibition and attenuation probabilities (percentage area of filled boxes, right; Methods). **c**, Focusing on one antibiotic in a stable three-species community, increasing the abundance of the yellow species creates negative feedback by decreasing the abundance of blue and red, which results in more inhibition of yellow. **d**, Communities are not stable at low levels of degradation due to positive feedback, whereby increasing the abundance of the yellow species results in a decrease of inhibition.



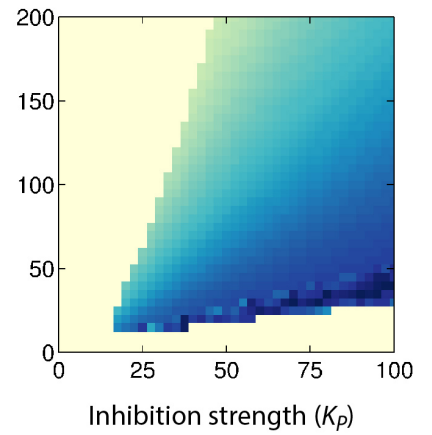
b Exponential inhibition
 $G_1 = R(x)g_1e^{-K_P C_3}$



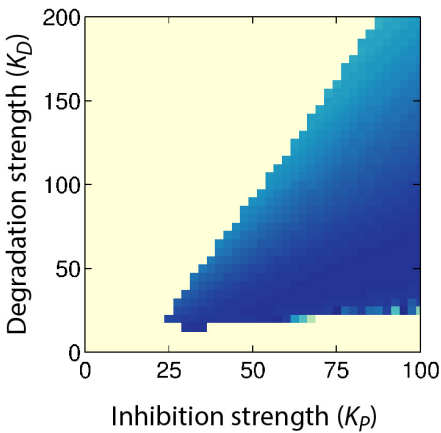
Monod inhibition
 $G_1 = R(x)g_1/(1 + K_P C_3)$



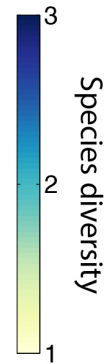
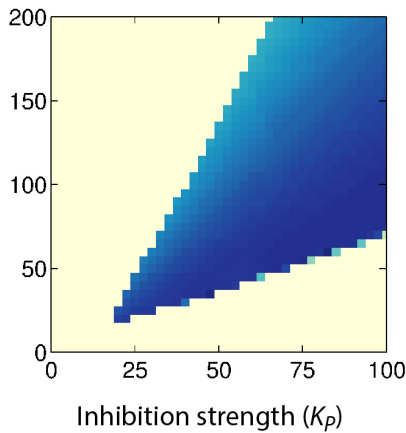
Linear Inhibition
 $G_1 = R(x)g_1 - K_P C_3$



Partial inhibition
 $G_1 = R(x)g_1(e^{-K_P C_3} + .2)/1.2$

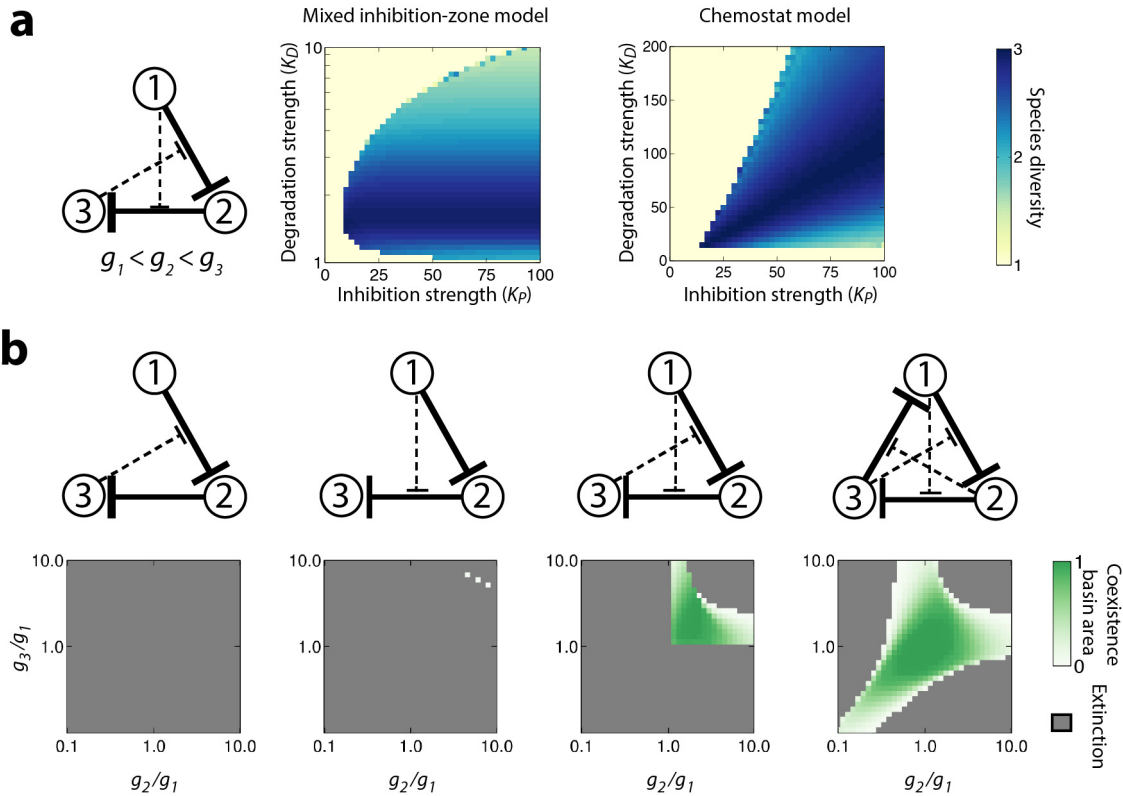


Diffuse interactions
 $G_1 = R(x)g_1e^{-K_P((C_1+C_2)/10+C_3)}$



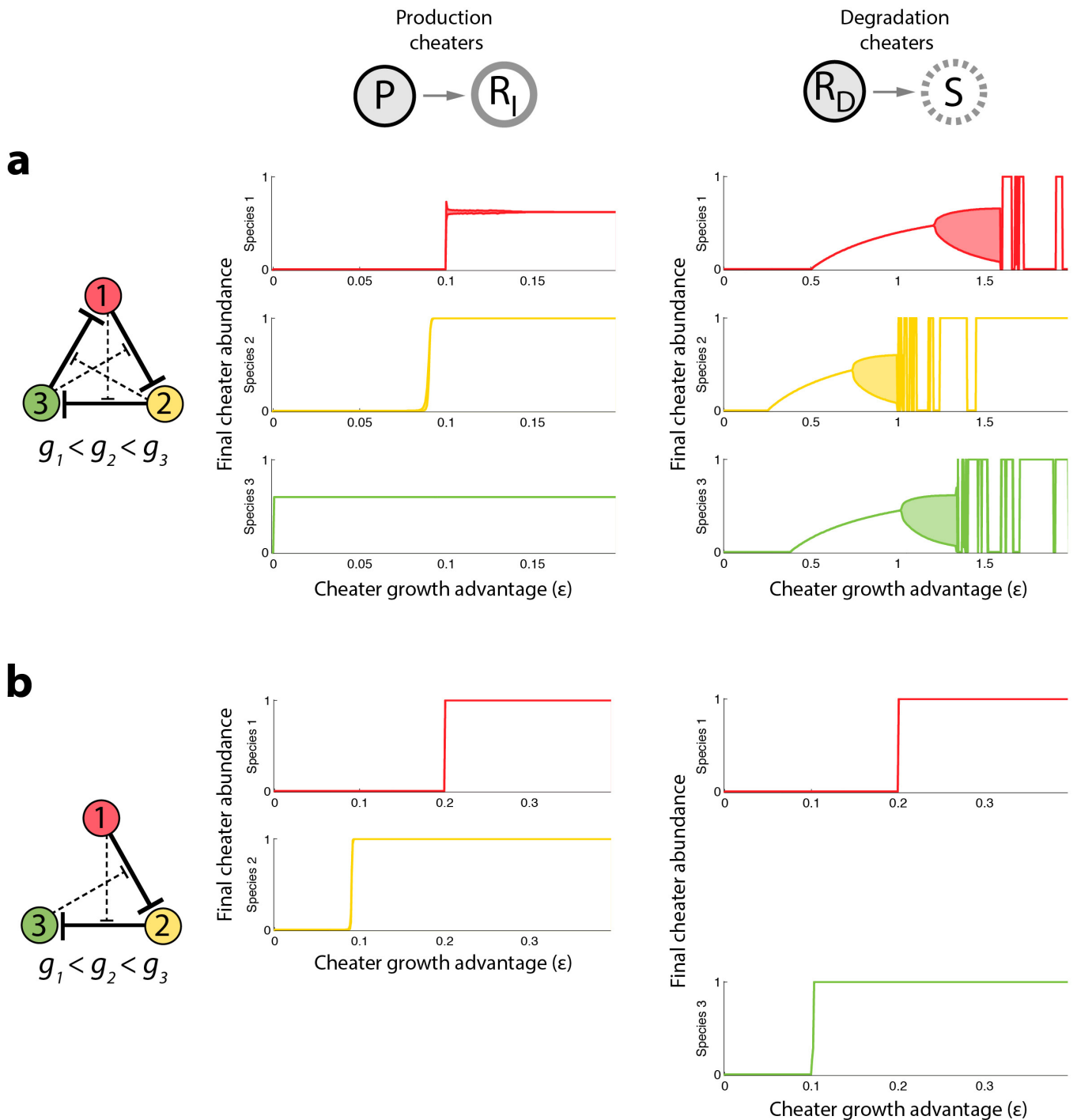
Extended Data Figure 5 | Coexistence of antibiotic degrading communities in a well-mixed chemostat model with three antibiotics. **a.** Stability of the three-species, three-antibiotic community in a single resource chemostat model in which species and antibiotics are completely homogeneous. Communities in the chemostat model may coexist through fixed points or limit cycles. For parameter sets in which the fixed point of the chemostat model was unstable, we started simulations close to the fixed point to determine if the community coexists through a limit cycle. Limit cycles occur in the areas between the dashed and solid black lines. Chemostat parameters: $g_1 = 3, g_2 = 6, g_3 = 9, k_2 = 0.5, P = 1$. **b.** Communities coexist in the chemostat for a wide range of assumptions regarding antibiotic mechanisms. We simulated the chemostat model while changing how the action of the antibiotics is modelled and

observed robust coexistence across all models. For each simulation we started all species at equal concentration ($X_i = 0.2$), ran the simulation until $t = 100$ generations and calculated the Shannon diversity of the final species levels. The default chemostat model assumes exponential inhibition of species by antibiotics, but similar coexistence is observed for Monod-like inhibition, for linear inhibition (for $G_i < 0$ we set $G_i = 0$), when species are only partially inhibited or when each species is sensitive at some level to all antibiotics. G_1 is the growth rate of species 1 under inhibition, while g_1 is its maximal rate of growth; $R(x)$ captures resource dependence on current species levels; C_1, C_2 and C_3 are the concentrations of antibiotics produced by species 1–3 respectively (Methods). Equations for the growth of species 2 and 3 have the same form as G_1 . All other parameters are the same as for panel **a**.



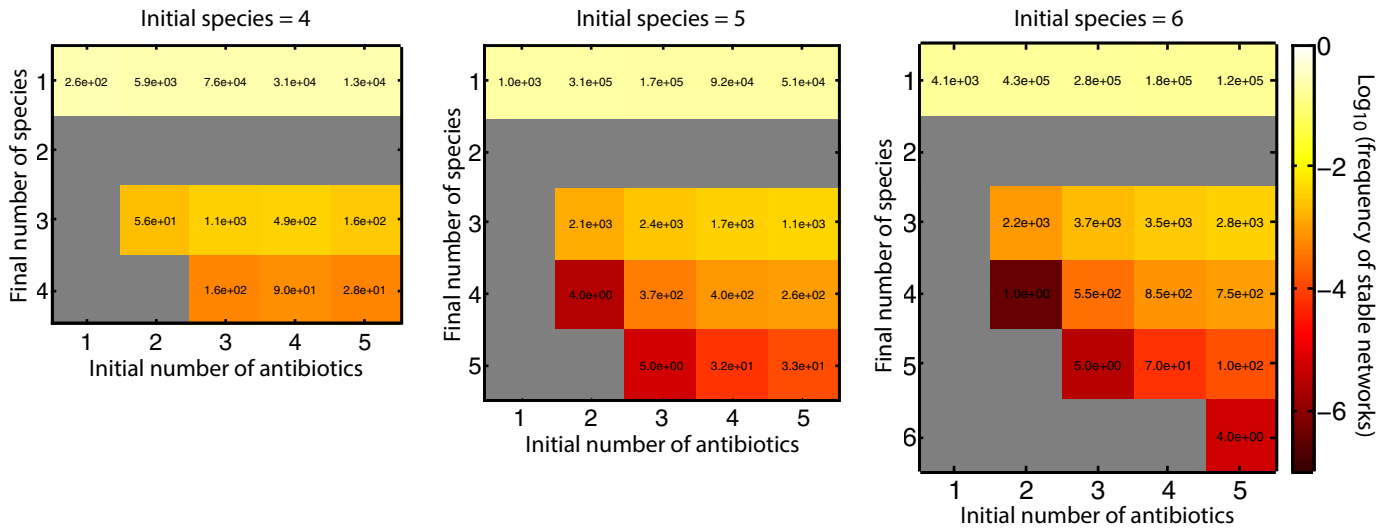
Extended Data Figure 6 | Coexistence of communities with three species and two antibiotics. **a**, Comparing community diversity in the mixed inhibition-zone model and the chemostat model. For each simulation we started all species at equal concentration ($X_i = 1/3$ for the inhibition-zone model, $X_i = 0.2$ for the chemostat model), ran the simulation for until $t = 100$ generations and calculated the Shannon diversity of the final species levels. Other parameters are the same as in Fig. 2 for the inhibition-zone model or Extended Data Fig. 5 for the chemostat model. **b**, Three species communities

require two antibiotics for stability. When only one antibiotic is degraded the community either lacks stability (first panel), or is stable only for a small number of growth rates and initial conditions (second panel). When two antibiotics are degraded the community is robustly stable to differences in species growth rates and initial conditions (third panel), provided that the antibiotics inhibit the faster-growing species (species 2 and 3). Basin colours as in Fig. 2b; grey shows parameters for which no initial conditions were stable; $K_p = 40$, $K_D = 4$.



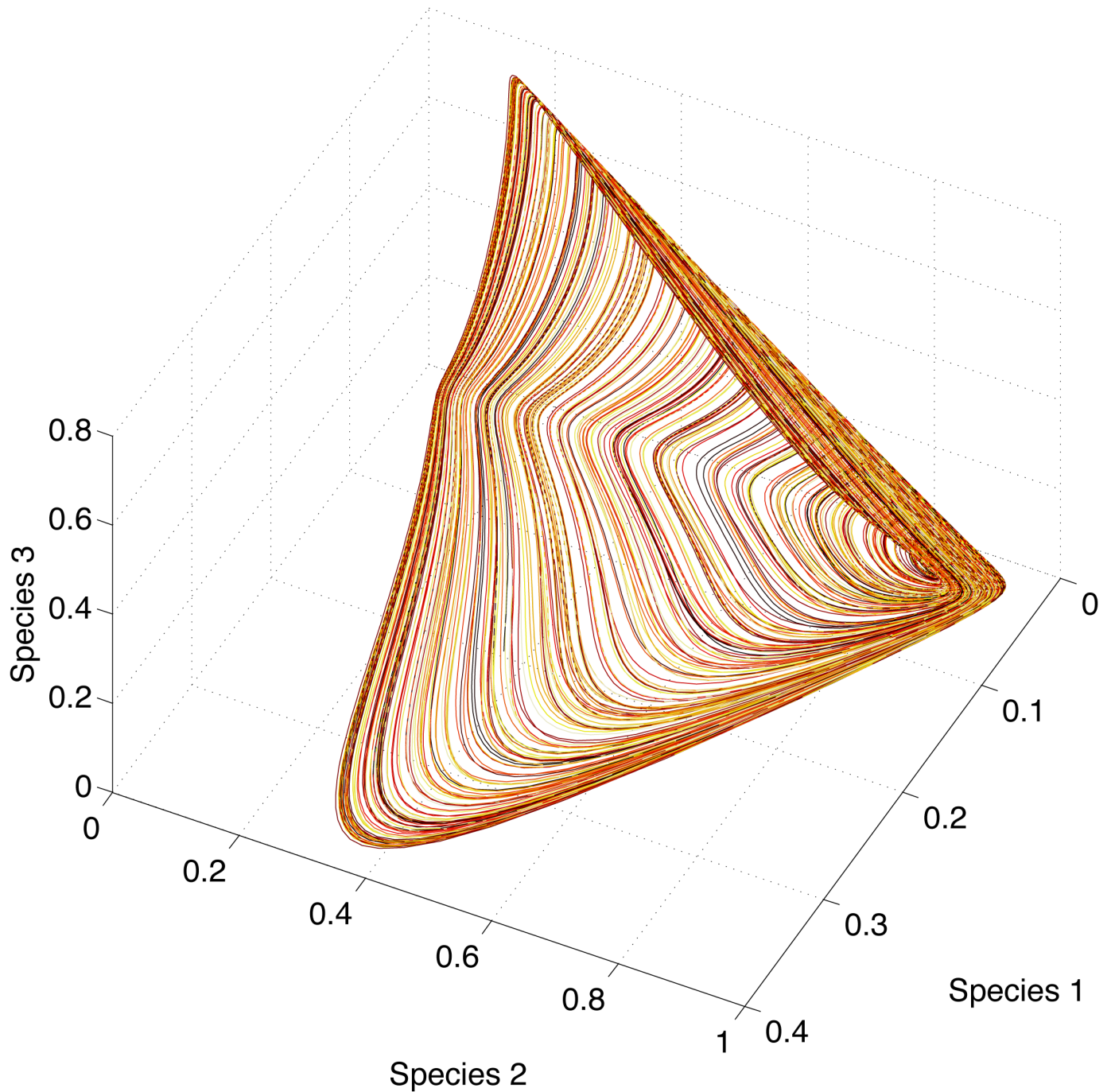
Extended Data Figure 7 | Robustness of three species communities to invasion by cheaters in the mixed inhibition-zone model. Analysis of production cheaters ($P \rightarrow R_1$, left) and degradation cheaters ($R_D \rightarrow S$, right). As in Fig. 3, we plot the final abundance of each cheater as a function of its growth advantage ϵ over its parent species. **a**, Cheaters cannot invade the three-species, three-antibiotic network when their growth advantage is small, except for the production cheater of the species with the fastest inherent growth rate (species 3, green line), which replaces its parent generating a new stable community of three species interacting through two antibiotics. **b**, This resulting three-species, two-antibiotic community is resilient to invasion by all cheaters; cheaters must have a substantial growth advantage to invade

and take over. Parameters for both networks are the same as Fig. 3. Shaded areas indicate the maximum and minimum abundance when the community reaches stable oscillations. Note, the analysis above is for networks with $g_1 < g_2 < g_3$. The alternative network of $g_1 > g_2 > g_3$, is less robust to invasion by production cheaters. Two cheaters can invade this community even with small ϵ : the production cheater for species 2 invades the network in **a** and gives rise to a stable three-species two-antibiotic community, while the production cheater for species 1 can take over the communities shown in **a** and **b**. For degradation cheaters this alternative network is similarly robust to cheaters as shown.



Extended Data Figure 8 | Complex network topologies support coexistence of larger numbers of species in the mixed inhibition-zone model. For given initial numbers of species and antibiotics, sets of up to 10^6 communities with random networks were simulated and the final number of surviving species recorded. The number inside each square shows how many networks resulted in the specified number of final species (after removing networks that did not

use all of the initial antibiotics, Methods). Colours show the frequency of each outcome within all simulated networks, with grey where no stable networks were found. We sparsely sampled parameters for species growth rates and antibiotic production and degradation levels (Methods). The sparse sampling means that a given network topology may exhibit stability for parameter combinations that were not tested.



Extended Data Figure 9 | A community with chaotic dynamics. Plotting the abundance of species 1–3 for the network from Fig. 4b. We show the last 30,000

steps of a simulation with 40,000 total generations, coloured with a slowly changing gradient. The trajectories form a strange attractor.

Extended Data Table 1 | Strain information for experimental assays

ED Fig. 1b ED Fig. 2	ED Fig. 1c	Species	Notes	Assays
p1		<i>Kutzneria sp. 744</i>	producer	1
p2		<i>Streptomyces clavuligerus</i> (ATCC 27064)	producer	1
p3		<i>Streptomyces sviveus</i> (ATCC 29083)	producer	1
p4		<i>Streptomyces sp. Mg1</i>	producer	1
p5		<i>Streptomyces albus</i> (J1074)	producer	1
m1		<i>Streptomyces SPB74</i>		1
m2		<i>Streptomyces griseoflavus</i> Tu4000		1
m3		<i>Streptomyces sp. AA#4</i>		1
m4	1	<i>Streptomyces pristinispiralis</i> (ATCC 25486)		1, 2, 3
m5		<i>Streptomyces hygrosopicus</i> (ATCC 53653)		1
m6		<i>Streptomyces SPB78</i>		1
m7		<i>Streptomyces ghanaensis</i> (ATCC 14672)		1
m8	2	<i>Streptomyces roseosporus</i> (NRRL 11379)		1, 2, 3
m9		<i>Streptomyces viridochromogenes</i> (DSM 40736)		1
m10		<i>Streptomyces lividans</i> (TK24)		1
m11		<i>Streptomyces sp. E14</i>		1
	3	<i>Streptomyces coelicolor</i>		2, 3
	4	<i>Streptomyces sp. G1-4</i> , JN020492	soil A	2, 3
	5	<i>Kitasatospora sp. G4-12</i> , JN020549	soil A	2, 3
	6	<i>Streptomyces sp. G2-6</i> , JN020526	soil A	2, 3
	7	Unclassified <i>Streptomycetaceae</i>	soil B	2, 3
	8	<i>Streptomyces sp. G4-8</i> , JN020545	soil A	2, 3
	9	<i>Streptomyces sp. G1-14</i>	soil A	2
	10	<i>Streptomyces sp. RI18-DHHV3</i>	soil B	2
	11	<i>Amycolatopsis sp.</i>	soil B, Actinobacteria	2, 3
	12	<i>Kribbella sp. NBRC 104208</i>	soil B, Actinobacteria	2, 3
	13	<i>Rhodococcus sp.</i>	soil B, Actinobacteria	2, 3
	14	<i>Microbacterium sp.</i>	soil B, Actinobacteria	2
	15	<i>Rhodococcus sp. 602</i>	soil B, Actinobacteria	2
	16	<i>Agromonas sp.</i>	soil B, Alphaproteobacteria	2, 3
	17	<i>Lysobacter sp.</i>	soil B, Gammaproteobacteria	2
	18	<i>Bradyrhizobiaceae Bosea</i>	soil B, Alphaproteobacteria	2
S		<i>E. coli</i> MC4100-YFP/pCS-I	assay strain w/ chromosomal YFP	1
	S	<i>E. coli</i> MC4100, pZS2R-YFP	assay strain w/ YFP plasmid	2, 3
	S	<i>E. coli</i> MC4100, pZS2R-CFP	assay strain w/ CFP plasmid	2, 3

Assay numbers: 1, three-species interaction assay; 2, antibiotic modulation assay; 3, β -lactamase inhibitor assay.